Surface magnetism of gallium arsenide nanofilms

Huan Lu, Jin Yu, and Wanlin Guo*

State Key Laboratory of Mechanics and Control of Mechanical Structures and Key Laboratory for Intelligent Nano Materials and Devices of MOE, Institute of Nano Science of Nanjing University of Aeronautics and Astronautics, Nanjing 210016, China

(Received 12 June 2017; revised manuscript received 21 August 2017; published 27 November 2017)

Gallium arsenide (GaAs) is the most widely used second-generation semiconductor with a direct band gap, and it is being increasingly used as nanofilms. However, the magnetic properties of GaAs nanofilms have never been studied. Here we find by comprehensive density-functional-theory calculations that GaAs nanofilms cleaved along the ⟨111⟩ and ⟨100⟩ directions become intrinsically metallic films with strong surface magnetism and the magnetoelectric effect. Surface magnetism and electrical conductivity are realized via a combined effect of charge transfer induced by spontaneous electric polarization through the film thickness and spin-polarized surface states. The surface magnetism of ⟨111⟩ nanofilms can be significantly and linearly tuned by a vertically applied electric field, endowing the nanofilms with unexpectedly high magnetoelectric coefficients, which are tens of times higher than those of ferromagnetic metals and transition-metal oxides.

DOI: 10.1103/PhysRevB.96.184430

I. INTRODUCTION

Magnetism originating from surfaces and interfaces is always related to strong correlated systems with unoccupied d or f electrons, and it has attracted a great deal of attention in device development. In the 20th century, this phenomenon was investigated intensively in magnetic metals and transition-metal oxides [1–5], and it was usually attributed to the Ruderman-Kittel-Kasuya-Yosida (RKKY) interaction [6–8] or spin-dependent exchange interaction [9–11]. In recent decades, the magnetic system has been extended to s and p hybrid electrons with the rise of low-dimensional materials [12–18]. In graphene, hexagonal boron nitride, and other two-dimensional crystals, magnetism can be induced by defects, structure distortions [19–21], as well as edge states [12,22,23]. Recently, ferromagnetism on reconstructed Si⟨111⟩ surfaces has been theoretically predicted, where the time-reversal symmetry is broken by the spontaneous surface reconstruction and magnetic instability [24]. Magnetic moments in metal oxides and perovskite materials caused by holes in oxygen p orbitals have also been widely predicted [25–30], and ferromagnetic ordering can be obtained if the hole density is high enough [25,26,30–32]. A representation is the polar (0001) oriented surfaces of wurtzite ZnO, in which local spin polarization of O atoms induced at the surface is three times larger than in the bulk [31], and the surface ferromagnetism can be considerably tuned via cobalt doping [31] or hydrogen adsorption [33]. Oxygen has a high electronegativity, thus the surface oxygen can easily achieve a high density of states at the Fermi level. However, it is challenging for other atoms on the surface to achieve that. One possible strategy is doping carriers to increase the density, and this has been realized in monolayer GaSe [34]. Charge transfer is another effective way to induce magnetism [35–39]. For example, an interfacial magnetism in $(LaNiO_3)n/(LaMnO_3)_2$ superlattices can be realized in $LaNiO_3$ with electrons transferring from $LaMnO_3$ to $LaNiO_3$ [39].

Usually, the surface magnetism can be tuned by a vertically applied electric field, which is called the surface magnetoelectric (ME) effect [40]. Up to now, almost 100 compounds have been studied to reveal the ME effect [41–43]. The underlying mechanisms of the ME effect can be classified into two categories. In ferromagnetic metal films and graphene nanoribbons [44–46], the ME effect results from the electric field-induced spin imbalance and exchange interaction. As for multi-ferroelectric or ferroelectric-ferromagnetic multilayers [47–51], the ME effect is by virtue of the piezoelectric strain in the ferroelectric constituent of the heterostructure, which would change the magnetic properties of the ferromagnetic constituent [52–54]. As ME effects in these materials are confined to the interfaces or surfaces, the relationship between the induced magnetization ($\Delta\mathbf{M}$) and external electric field ($\mathbf{E}$) can be expressed as

$$\mu_0 \Delta\mathbf{M} = \alpha\mathbf{E}, \tag{1}$$

where μ_0 denotes the magnetic permeability of vacuum and α denotes the surface or interface ME coefficient.

In addition to changing magnetic properties, surface states can also distinguish nanofilms from their bulk materials in electrical conductivity. The electronic reconstruction at the surface or interface can give rise to a highly conductive property [55–58], and sometimes it combines with magnetism [57,58]. A representative case in this area is cubic boron nitride (BN) ⟨111⟩ nanofilms [59]. In contrast to intrinsic electrical insulation of BN materials, the BN nanofilms become metallic due to the labile near-gap states originating from the surface.

As an important second-generation semiconductor, GaAs is nonmagnetic with a direct band gap of 1.43 eV, and it has been increasingly used as nanofilms [60]. Doping magnetic atoms to bulk GaAs leads to diluted magnetic semiconductors [61–65]. After more than a decade of effort, the Curie temperature of the best diluted magnetic semiconductors, (Mn,Ga)As, was raised to almost 200 K [66]. Magnetic atoms on GaAs surfaces can also result in various magnetic properties [67–69], with the magnetic anisotropy energy being a function of the cluster size for an individual Mn impurity positioned in the vicinity of the ⟨110⟩ GaAs surface [67]. Nonetheless,

*wlguo@nuaa.edu.cn

intrinsic surface states in GaAs nanofilms have never been reported. In this study, we find that GaAs nanofilms cleaved along the ⟨111⟩ and ⟨100⟩ directions become intrinsically metallic films with strong surface magnetism and the ME effect. With charge-transfer normal to the nanofilms, excess screening charge confined to a depth of a few atoms from the surface leads to the intrinsic metallicity of the whole structure. Due to exchange interactions, the screening charge is spin-dependent, exhibiting surface magnetism. Once these nanofilms are exposed to a vertically applied electric field, the spin dependence of the screening electrons leads to a strong ME effect. Since the electric field hardly penetrates into midlayers of GaAs nanofilms, the ME effect is limited to the surface as a surface ME effect.

II. CALCULATION METHOD

All calculations are carried out based on density-functional theory (DFT) in the Vienna *ab initio* simulation package (VASP) [70,71]. The studied systems are free-standing fcc GaAs⟨111⟩ nanofilms and fcc GaAs⟨100⟩ nanofilms with periodic boundary conditions. The Kohn-Sham equation was solved iteratively using a plane-wave basis set with a cutoff energy of 500 eV to describe the valence electrons. The exchange correlation effects were incorporated in the spin-polarized generalized gradient approximation (GGA) using the Perdew-Burke-Ernzerhof (PBE) functional, and the electron-ion interactions were described by the projector augmented wave (PAW) method [72]. For the hexagonal unit cell, the Brillouin-zone sampling was performed using a $15\times15\times1$ MP grid for atomic structure relaxation calculations and a $30\times30\times1$ MP grid for static calculations [73]. All of the atoms in the unit cell were fully relaxed until the force on each atom was less than 0.001 eV/Å. Electronic minimization was performed with a tolerance of 10^{-5} eV. The vacuum between two adjacent planes was larger than 15 Å to separate the interaction between periodic images. The uniform external electric field applied perpendicular to the nanofilm surface was introduced by the planar dipole layer method as implemented in VASP [74]. The dipole correction [75] is adopted to set the electric field in the vacuum region to zero.

III. RESULTS AND DISSCUSIONS

The nanofilms are cleaved along the ⟨111⟩ and ⟨100⟩ directions of the cubic GaAs structure without passivation, the unit cells of which are a standard rhombus with an optimized lattice constant of $a = b = 3.997$ Å and quadrate with $a = b = 4.093$ Å. The thickness of nanofilms is defined as the cleaved monolayer (ML) number n indexed by a subscript, and each monolayer contains one layer of Ga and one layer of As. For example, $Ga_5As_5\langle111\rangle$ or $\langle111\rangle_5$ nanofilm represents for the nanofilm cleaved along the ⟨111⟩ direction with five ML ($n = 5$), which contains five Ga atoms and five As atoms. The outermost surface with a Ga atom is denoted as the top surface, and the outmost surface with an As atom is denoted as the bottom surface. First of all, the stability of the nanofilms is confirmed by quantum

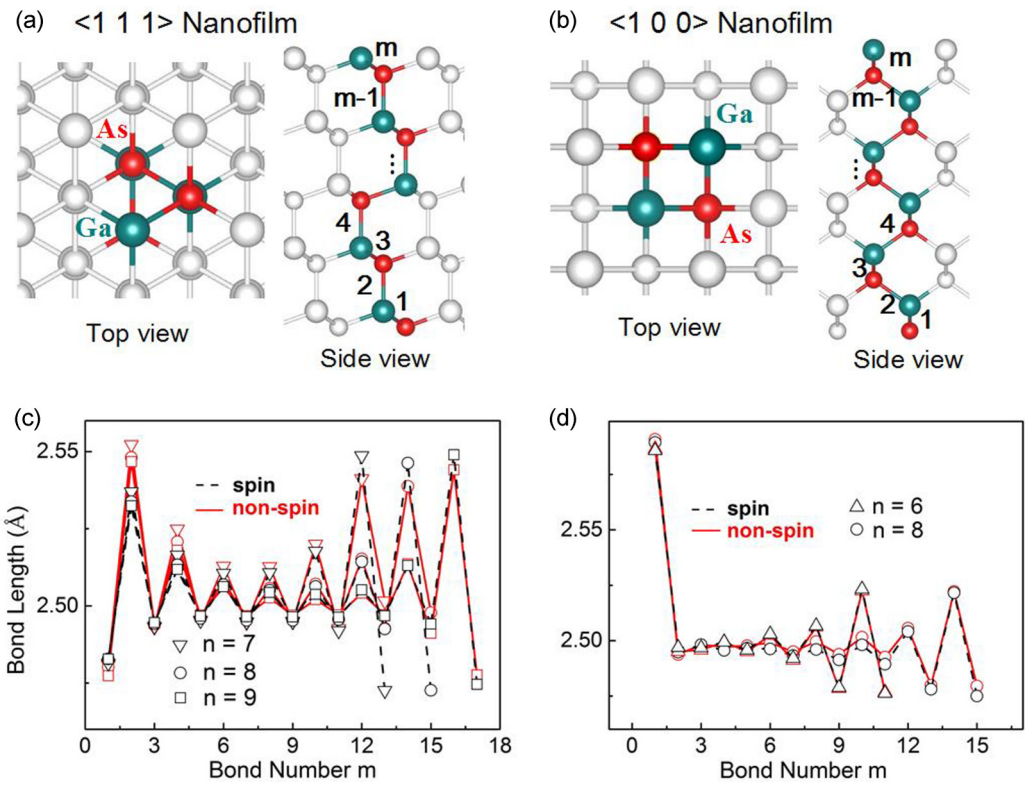

FIG. 1. Structural properties of GaAs nanofilms. The top view (left) and side view (right) of the atomic structures of the unit cells of (a) ⟨111⟩ and (b) ⟨100⟩ nanofilms, where m indexes the bond number in the nanofilms. (c),(d) Bond length of ⟨111⟩ and ⟨100⟩ nanofilms along the ⟨001⟩ direction, respectively.

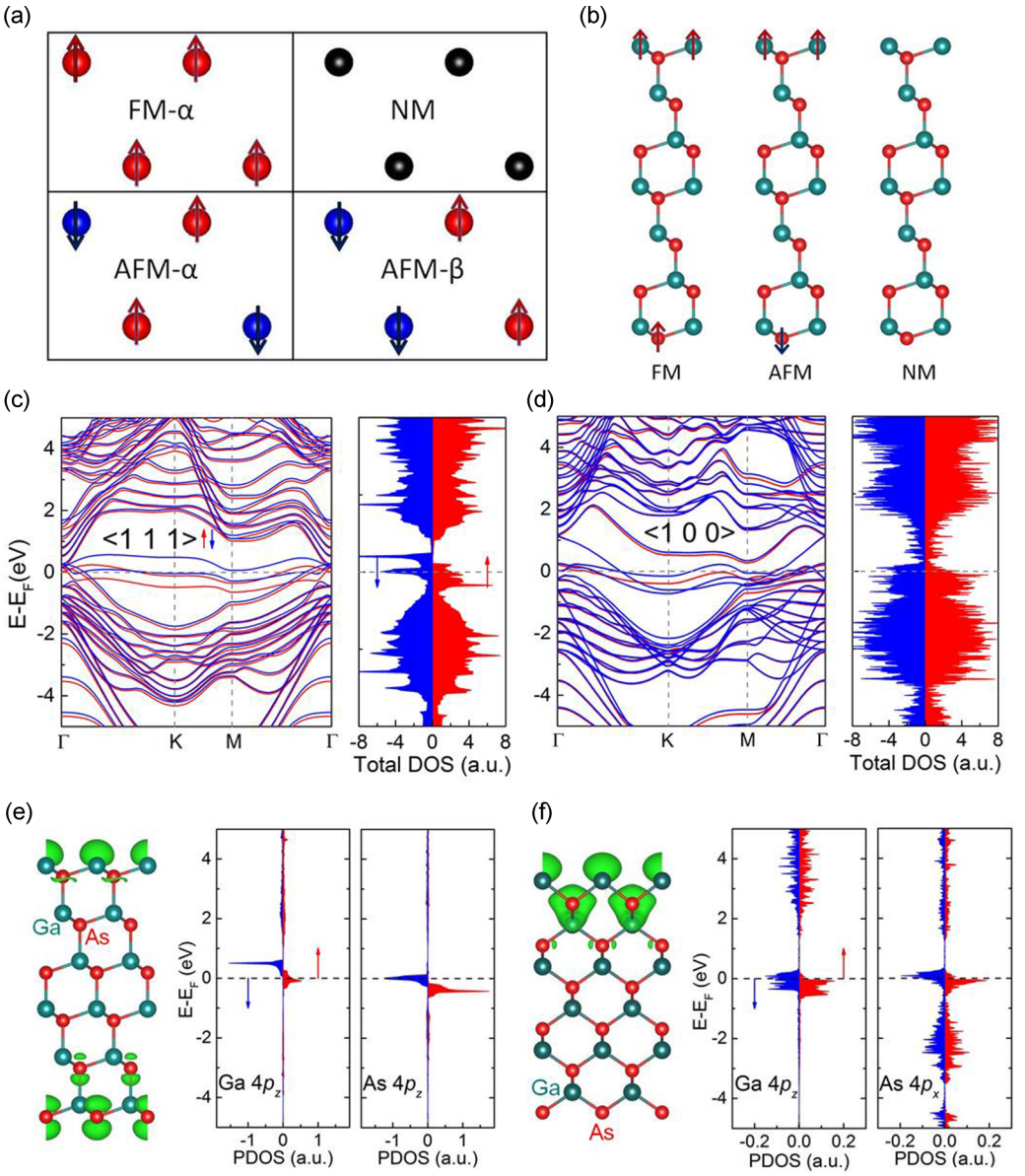

FIG. 2. Magnetic structure and electronic properties of GaAs nanofilms. (a) Top view of the different in-plane spin configurations in ⟨111⟩ nanofilms for the FM-α, NM, AFM-α, and AFM-β states, with only the outmost atoms being shown. (b) Side view of the different intersurface spin configurations in $\langle 111\rangle_7$ nanofilms for the FM, AFM, and NM states. (c),(d) Spin-polarized band structure and total density of states in $\langle 111\rangle_6$ and $\langle 100\rangle_6$ nanofilms. (e), (f) Spin-polarized electron distribution and projected density of states of the outmost Ga and As atoms of $\langle 111\rangle_6$ nanofilm and $\langle 100\rangle_6$ nanofilm, respectively. Spin directions are represented by arrows and colors (red for up and blue for down).

ab initio molecular-dynamics calculations; see Fig. S1 of the Supplemental Material [76]. Actually, the energetic and dynamical stability of single-layer III-V materials has been confirmed by first-principles calculations [77]. Optimized atomic structures of one unit ⟨111⟩ and ⟨100⟩ nanofilms are colored and presented in Figs. 1(a) and 1(b), and their bond lengths are analyzed in Figs. 1(c) and 1(d). The surface atoms of ⟨111⟩ nanofilms have little fluctuation, and the bond length of surface layers varies much more than that of the midlayers for n from 7 to 9. It is obviously that the bond lengths of ⟨111⟩ nanofilms change around the value of bulk GaAs (2.50 Å in our simulations) even in the center of the slab as thick as 9 ML. As presented in Fig. 1(a), those bonds almost perpendicular to the nanofilms are slightly shorter than the remaining ones because of the built-in electric field along the thickness direction of the films, as will be shown below. Further, when spin polarization is taken into account, the bond length of the outmost Ga and the closest As atoms changes slightly, rendering a more undulating top surface. The bond length of ⟨100⟩ nanofilms undergoes a similar change to that shown in Fig. 1(d). It is energetically more favorable to form planar nanosheets for GaAs nanofilms thinner than 3 ML, like many wurtzite nanostructures being reported [78,79]. Therefore, we focus on the magnetic properties of those thicker nanofilms.

First of all, we consider the ferromagnetic states of ⟨111⟩ nanofilms, in which all atoms have the same spin direction. The results show surface magnetism in Fig. 2(e), and the in-plane magnetism of the two outermost surface layers

contributes the vast majority of magnetic moments in the entire nanofilm. To determine the most stable in-plane spin orderings of these outermost surface layers, we set different in-plane spin configurations for each layer individually, and the magnetic moments of the rest atoms are all set to zero in the meanwhile. There are four possible magnetic ground states being considered in one outermost layer of 2×2 supercells: nonmagnetic (NM), ferromagnetic (FM)-α, antiferromagnetic (AFM)-α, and AFM-β, as shown in Fig. 2(a). The FM-α state is the most favorable in-plane magnetic state in energy for all the cases considered in this work. For the outermost Ga layer of the top surface of $Ga_5As_5\langle 111\rangle$ nanofilm, the ground-state energy of the FM-α state is 23.1, 21.0, and 20.9 meV per atom lower than that of the NM, AFM-α, and AFM-β states, respectively. For the outermost As layer of the bottom surface of $Ga_5As_5\langle 111\rangle$ nanofilm, the ground-state energy of the FM-α state is 18.3, 16.2, and 16.2 meV per atom lower than that of the NM, AFM-α, and AFM-β states, respectively. For $\langle 111\rangle$ nanofilms thicker than 3 ML, the energy difference between FM-α and NM states increases from 0 at 3 ML to around 20 meV per atom at 5 ML, and it remains unchanged with further increasing n. The energy difference between FM-α and two AFM states shows the same trend. For $\langle 100\rangle$ nanofilms, the ground states of the top surface and the closest As layer are also found to be ferromagnetic, and the ground-state energy is around 25 and 17 meV per atom lower than that of the NM and two AFMs, respectively.

The exchange interaction between the two outermost surfaces of $\langle 111\rangle$ nanofilms is considered as well. The two outermost magnetic layers have the same spin direction as denoted by FM, or different spin directions as denoted by AFM in Fig. 2(b). The energy differences between the FM and AFM or NM states are shown in Table I, where $\Delta E_{f\text{-}n} = E_{\mathrm{FM}} - E_{\mathrm{NM}}$ and $\Delta E_{f\text{-}a} = E_{\mathrm{FM}} - E_{\mathrm{AFM}}$ per unit cell as shown in Figs. 1(a) and 1(b), respectively. E_{FM}, E_{AFM}, and E_{NM} represent the total energy of FM, AFM, and NM states per unit cell, respectively. FM coupling between two surface states of the magnetic nanofilms thicker than 3 ML is the ground state. Both $\Delta E_{f\text{-}n}$ and $\Delta E_{f\text{-}a}$ have a sudden decrease with increasing n from 3 to 5, and then they become relatively stable. For the $\langle 100\rangle$ case, FM is the ground state as well, and the top and subtop surfaces of the nanofilm contribute the most magnetic moment, which is different from the $\langle 111\rangle$ nanofilms. The coupling between these two magnetic layers is much stronger than that of $\langle 111\rangle$ nanofilms since the two magnetic layers of $\langle 100\rangle$ nanofilms are located next to each other, as shown in Fig. 2(f).

TABLE I. The energy difference per unit cell, as shown in Figs. 1(a) and 1(b), between the FM (the spins in two magnetic layers have the same direction) and NM states ($\Delta E_{f\text{-}n}$), the energy difference per unit cell between the FM and AFM (the spins in the two magnetic layers have different directions) states ($\Delta E_{f\text{-}a}$), and the total magnetic moments (MM) per unit cell of $\langle 111\rangle$ and $\langle 100\rangle$ nanofilms with various thicknesses.

	$\langle 111\rangle_3$	$\langle 111\rangle_4$	$\langle 111\rangle_5$	$\langle 111\rangle_9$	$\langle 111\rangle_{15}$	$\langle 100\rangle_8$
$\Delta E_{f\text{-}n}$ (meV)	20.4	−6.4	−43.4	−47.7	−39.4	−56.0
$\Delta E_{f\text{-}a}$ (meV)	20.2	−1.2	−7.8	−9.5	−6.8	−20.1
MM (μ_B/a.u.)	0	0.544	0.896	1.342	1.381	0.438

The total magnetic moment of the unit cell with the FM state, as shown in Table I, has the same trend of $\Delta E_{f\text{-}n}$ and $\Delta E_{f\text{-}a}$ when n increases since the denser surface states, which will be discussed below, always lead to a stronger and more stable surface magnetism. The contributions of the top and bottom surfaces to the total magnetic moment of the unit cell are almost the same. For $\langle 111\rangle_5$ nanofilm, the magnetic moments of the top and bottom surfaces are 0.436 μ_B and 0.459 μ_B, respectively. The magnetic moments of the top or bottom surfaces of the nanofilms with different thicknesses are all approximately half of the total magnetic moment of the entire nanofilm.

As the total density of states (DOS) of spin-polarized calculation shown in Figs. 2(c) and 2(d), both up- and down-spin electrons induced by spin polarization concentrate in the energy window of −1 and 1 eV, and they are degenerated around the Fermi level (E_F). Different from the cubic GaAs structures showing semiconducting characters, nanofilms of GaAs are all ferromagnetic metals with flat bands crossing through the E_F. By visualizing the magnetization density in Figs. 2(e) and 2(f), we found the degenerated DOS in GaAs nanofilms originating from the strong localized states of the

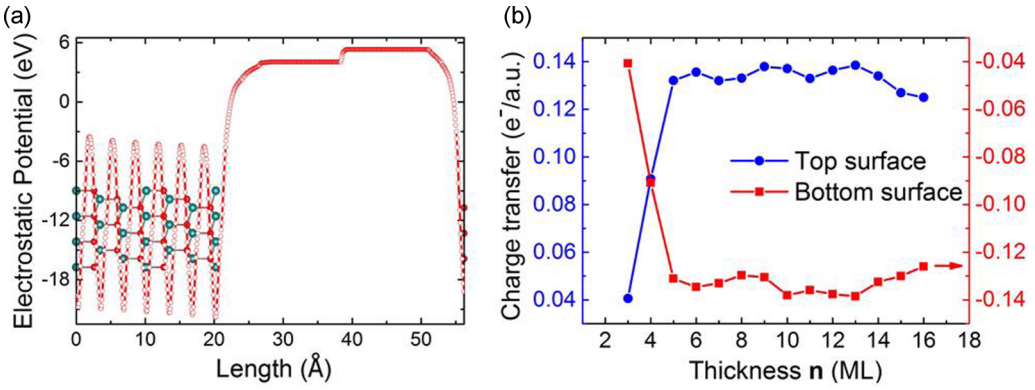

FIG. 3. Built-in electric field and charge transfer in the $\langle 111\rangle$ nanofilms. (a) Plane-averaged electrostatic potential along the normal direction of $Ga_7As_7\langle 111\rangle$ nanofilm. (b) The total charge transfer between the Ga (blue) and As (red) surfaces as a function of thickness. For the top (bottom) surface, the transferring charge is represented by the sum of variations of valence electrons in four atoms, which are four nearest atoms from the top (bottom) surface in the unit cell.

outermost atoms with an almost entire unpaired electron wave function in p character. For $Ga_6As_6\langle 111\rangle$ nanofilm, further analysis on the projected DOS of the outermost Ga and As atoms in Fig. 2(e) shows that spin-polarized electrons of the $4p_z$ orbital in the outermost Ga atom present a large splitting energy of 0.598 eV, and that of the $4p_z$ orbital in the outmost As atom is 0.448 eV, rendering the imbalance redistribution of spin-polarized electrons at the surfaces. The degenerated DOS induced by the split $4p_z$ orbital of the outermost atoms is also observed in the outermost Ga atom of $Ga_6As_6\langle 100\rangle$ nanofilm, and the closest As to the top surface has a large splitting energy of the $4p_x$ and $4p_y$ orbitals as well, with a corresponding splitting energy of 0.161 eV for the $4p_z$ orbital of Ga, and 0.160 and 0.165 eV for the $4p_x$ and $4p_y$ orbitals of As, respectively. Figure 2(f) shows the results of $Ga_6As_6\langle 100\rangle$ nanofilm, and only the $4p_x$ orbital of As is presented since the $4p_y$ orbital has a similar DOS with $4p_x$; see Fig. S2 of the Supplemental Material [76].

To elucidate the origin of the large spin splitting, we plot the plane-averaged electrostatic potential along the normal of $Ga_7As_7\langle 111\rangle$ nanofilm in Fig. 3(a). A linear distribution of the electrostatic potential is induced by electric polarization, which means a built-in electric field pointing from the top surface to the bottom surface. The averaged potential difference between the outermost atoms at the top surface and the bottom surface is estimated to be 1.302 eV. The plane-integrated charge transfer between two surfaces upon formation of the nanofilm as a function of thickness is shown in Fig. 3(b). To avoid the effect of isolated atoms, the charge transfer of each surface is represented by the sum of variations of valence electrons in four atoms, which are located in the surface and subsurface of the unit cell. The analysis reveals that for the top (bottom) surface, all four nearest atoms receive (lose) extra valence electrons compared to their bulk values. Therefore, electrons are indeed depleted at the bottom surface atoms and accumulate at the top surface atoms. There are at least $0.12e^-$ transferring from the bottom surface to the top surface after a sudden jump with increasing n from 3 to 5 due to the built-in electric field. The sudden change is the formation process of spontaneous electric polarization with increasing thickness of the nanofilms. An inspiring study has revealed the thickness dependence of carrier density of the two-dimensional electron gas in $SrTiO_3$ (111) nanofilms [80]. Usually, to satisfy the Stoner criterion, a high density of states at the Fermi level is difficult to realize. However, in GaAs$\langle 111\rangle$ nanofilms, carriers at the Fermi level are dense enough at both the top and bottom surfaces due to the coexistence of unsaturated dangling bonds and the charge transfer, which makes it an excellent candidate for realizing ferromagnetism. Different from oxygen surfaces of metal oxides and perovskite materials [25–30], whose high density of states around the Fermi level is only contributed by the p orbitals because of the unsaturated dangling bonds, both s and p orbitals of surface atoms in GaAs$\langle 111\rangle$ nanofilms are spin-polarized, as shown in Fig. 2(e), because of the extra contribution from the transferring charge. For GaAs $\langle 100\rangle$ nanofilms, the magnetic moments mainly reside in the top surface, and their origin is related to the existence of p electrons of well-defined spin polarization.

Considering that spin-polarized electrons at surfaces are driven by the electric polarization across the nanofilms, we further apply the vertical electric field as shown in Fig. 4(a), which can modulate the electron transfer and tune the magnetic properties of the nanofilms. Here, we mainly focus on the ME effect in GaAs$\langle 111\rangle$ nanofilms. Our results reveal perfect linear ME effects in $\langle 111\rangle$ nanofilms, as shown in Fig. 4(b). By fitting the calculated data, the obtained ME coefficient α in Eq. (1) is

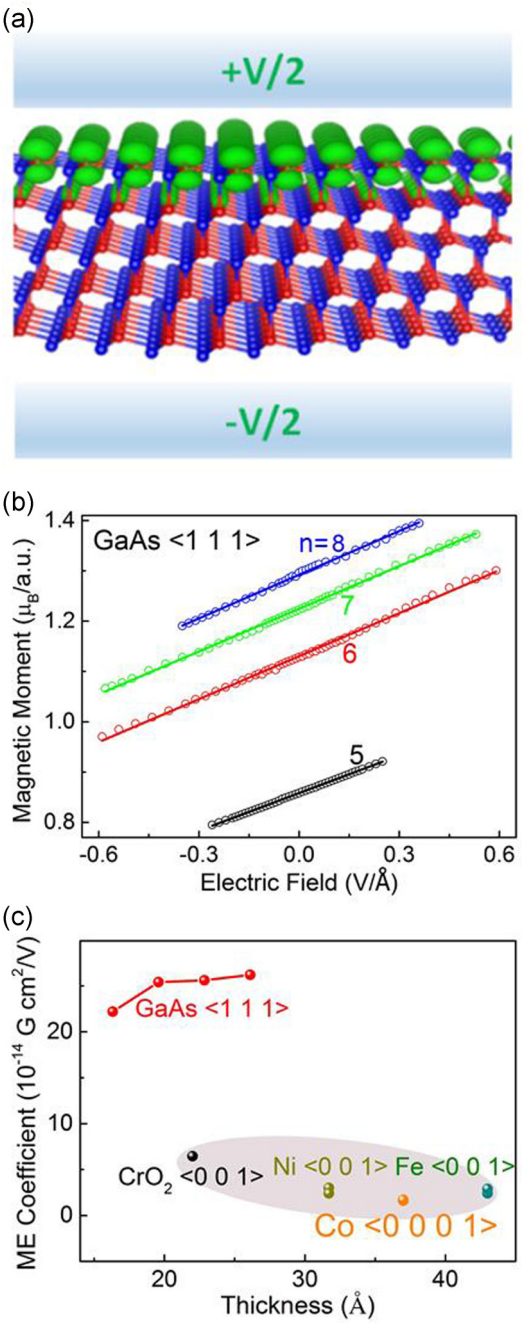

FIG. 4. ME effect in GaAs$\langle 111\rangle$ nanofilms. (a) Schematic diagram of the nanofilms under a vertically applied electric field. (b) External electric field induces linear magnetic polarization in $\langle 111\rangle$ nanofilms. The circle with different colors represents nanofilms with various thicknesses, and the solid line indicates the fitted date of the magnetic moment in the nanofilms. (c) Comparison of the ME coefficient in this study and previous reported ferromagnetic metal and transition-metal oxide nanofilms (Refs. [44,46]).

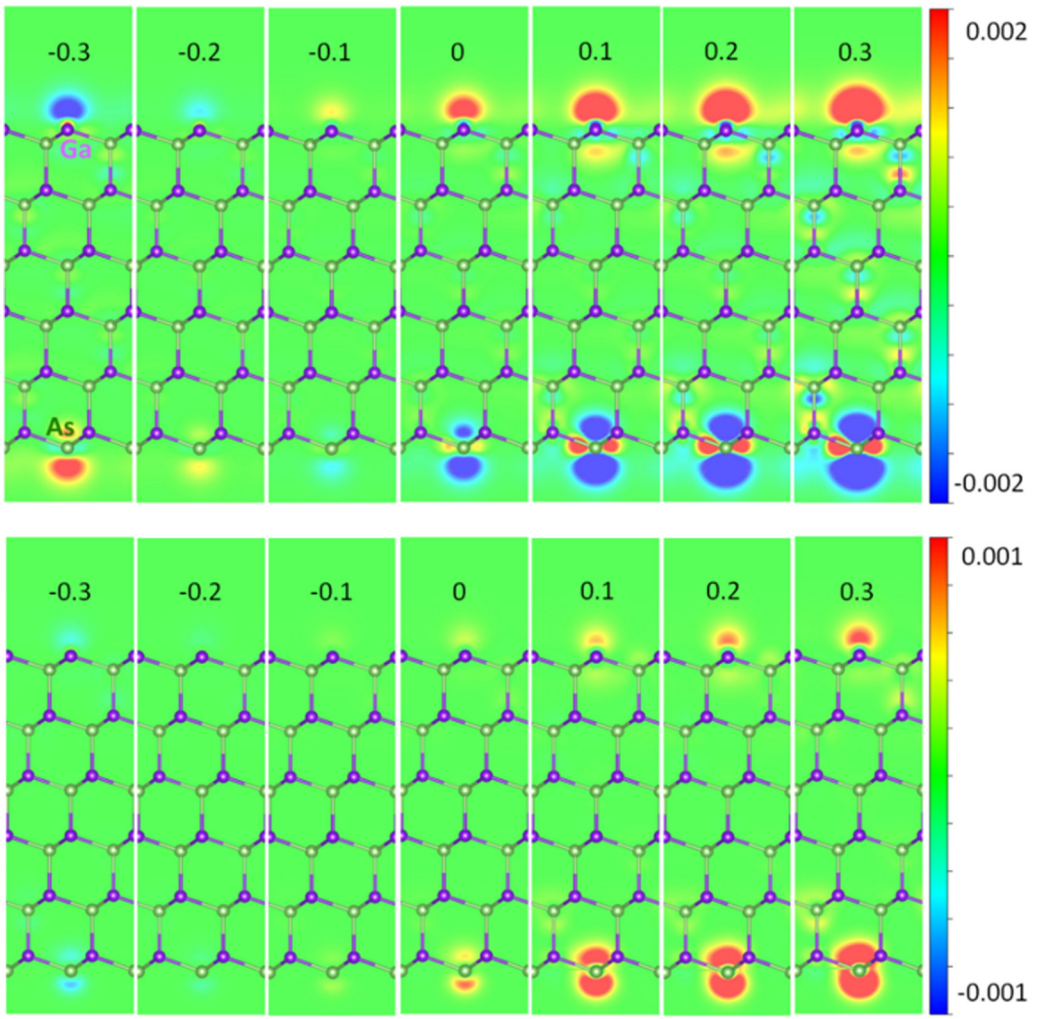

FIG. 5. Electric-field modulation of transferring charge and spin density in $Ga_6As_6\langle 111\rangle$ nanofilm. Side view of the differential charge (top panel) and spin-polarized electrons (bottom panel) under a vertically applied electric field ranging from -0.3 to 0.3 V/Å. Blue and red indicate electron depletion and accumulation, respectively.

in the magnitude of 10^{-13} G cm^2/V, which suggests that the surface magnetism in $\langle 111\rangle$ nanofilms is highly sensitive to an externally applied electric field. When the field increases from -0.6 to 0.6 V/Å, the magnetic moment of $Ga_6As_6\langle 111\rangle$ increases from $0.960\,\mu_B$ to $1.310\,\mu_B$. For nanofilms with thickness varying from 5 to 8 ML, the corresponding ME coefficient (in units of 10^{-13} G cm^2/V) is estimated to be $\alpha =$ 2.22, 2.54, 2.56, and 2.57, respectively. The ME coefficient of $\langle 111\rangle$ nanofilms is tens of times higher than those obtained at the ferromagnetic metal Co and Fe films [44]; see Fig. 4(c). Thereby, $\langle 111\rangle$ nanofilms are of greater potential in spintronic devices than traditional ferromagnetic metals. The high ME coefficient of $\langle 111\rangle$ nanofilms is reasonable because it has a small plane-averaged electrostatic potential, which makes its surface magnetism much easier to tune. Since the surface magnetism is mainly accounted for by the outermost surfaces atoms, the ME coefficient hardly changes with increasing thickness of $\langle 111\rangle$ nanofilms. As for $\langle 100\rangle$ nanofilms, the surface magnetism also varies monotonously with the external electric field (see Fig. S3 of the Supplemental Material [76]), but it cannot show a linear relationship.

The surface magnetism in $\langle 111\rangle$ nanofilms is due to the transferring charge and spin-polarized electrons at surfaces, and the redistribution of electrons under the external electric field contributes to the linear ME effect. Therefore, we present the differential charge $\Delta\rho$ of $Ga_6As_6\langle 111\rangle$ nanofilm in Fig. 5 to show the redistribution, where the differential charge is defined as $\Delta\rho = \rho_e - \rho_0$ (ρ_e and ρ_0 are the charge density of $Ga_6As_6\langle 111\rangle$ nanofilm with and without electric field, respectively). For a field of 0, redistribution of transferring charge originates from the spontaneous polarization across the nanofilm. When an external electric field is applied, the static equilibrium of transferring charge is broken. Under a positive electric field (parallel to the built-in electric field), electrons will deplete (concentrate) at the bottom surface (the top surface) atoms, and the transferring electrons from the bottom surface to the top surface increase as the electric field strength increases. In contrast, when a negative electric field is applied (antiparallel to the built-in electric field), electrons transfer from the outermost Ga atoms to the outermost As atoms. Further analysis on the spin-density difference reveals that those transferring electrons are not contributed equally to

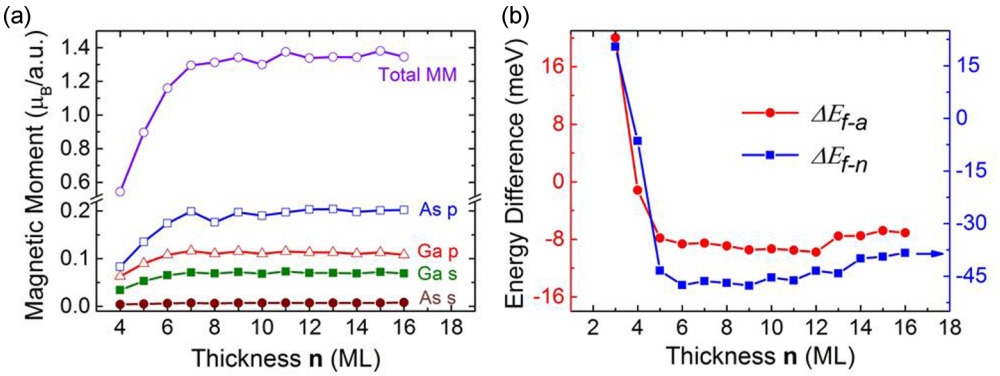

FIG. 6. Thickness dependence of surface magnetism and relative stability in ⟨111⟩ nanofilms. (a) The thickness dependence of magnetic moments of ⟨111⟩ nanofilms and different orbitals in terminal atoms. (b) The energy difference between the NM and FM states (blue solid) and the energy difference between the AFM and FM states (red circle).

the up- ($n^{\uparrow}$) and down-spin ($n^{\downarrow}$) electrons. Under a positive electric field, transferring electrons mainly occupy the p orbital as up-spin electrons, and the occupied electrons increase with increasing electric field strength; under a negative electric field, transferring electrons occupy the p orbital as down-spin electrons and the occupied electrons decrease as the electric-field strength decreases. Since the magnetization density is defined as the difference between $n^{\uparrow}$ and $n^{\downarrow}$, the total magnetic moment will increase monotonously with increasing electric field.

As shown in Fig. 6(a), surface magnetism in GaAs nanofilms is thickness-dependent. For ⟨111⟩ nanofilms, both the total magnetic moment and projected magnetizations are relatively stable when n increases beyond 7. Meanwhile, $\Delta E_{f\text{-}n}$ and $\Delta E_{f\text{-}a}$ have a sudden decrease with increasing n from 3 to 5, and then they become relatively stable, as shown in Fig. 6(b). The constant of $\Delta E_{f\text{-}n}$ and the magnetic moment in thicker nanofilms is understandable because the saturation of transferring charge is reached, and the initial thickness dependence of $\Delta E_{f\text{-}n}$ and the magnetic moment can be explained by the thickness dependence of the charge transfer, as shown in Fig. 3(b). As for the thickness-dependent $\Delta E_{f\text{-}a}$, long-ranged interlayer coupling between two surfaces should be considered. Recently, the importance of overlooked long-ranged interactions between magnetic ions has been revealed theoretically and experimentally in both monolayers [81] and van der Waals crystals [82–84]. The ⟨111⟩ nanofilm of 3 ML is an antiferromagnet with two surfaces having opposite spin directions due to significant contribution from interlayer superexchange interaction. For nanofilms thicker than 4 ML, the surface states decouple and the $\Delta E_{f\text{-}a}$ may be contributed from the transferring charge between surfaces. A clear piece of evidence is that applying every 0.2 V/Å positive electric field (parallel to the built-in electric field) would lead to about a 4 meV decrease in $\Delta E_{f\text{-}a}$, indicating a more stable FM configuration. Due to the limited computational ability, the thickest nanofilm in our simulations is 5.0 nm ($Ga_{16}As_{16}$⟨111⟩) with the magnetic moment up to 1.355 μ_B. The projected magnetization of the outermost Ga and As atoms shown in Fig. 6(a) further confirms that the p orbital of terminal atoms is the main contributor to the surface magnetism. The variation of the surface magnetism in ⟨100⟩ nanofilms shows the same trend but with a much smaller amplitude, as shown in Fig. S4 of the Supplemental Material [76].

IV. CONCLUSIONS

In summary, our first-principles calculations predict the existence of surface magnetism in metallic GaAs⟨111⟩ and ⟨100⟩ nanofilms. The surface magnetism is attributed to the imbalance of spin-polarized electrons near the Fermi level. A built-in electric field induced by electric polarization drives electrons transferring between the two outermost surfaces, and it plays an important role in realizing and retaining the surface magnetism. Under a perpendicular electric field, the surface magnetization of the nanofilms changes significantly with the field strength, exhibiting a strong linear magnetoelectric effect with high coefficients in the GaAs⟨111⟩ nanofilms.

ACKNOWLEDGMENTS

This work was supported by National Natural Science Foundation of China (Grants No. 51535005 and No. 51472117), the Fundamental Research Funds for the Central Universities (NP2017101), and a Project Funded by the Priority Academic Program Development of Jiangsu Higher Education Institutions.

[1] U. Gradmann, J. Magn. Magn. Mater. **6**, 173 (1977).
[2] S. Ohnishi, A. J. Freeman, and M. Weinert, Phys. Rev. B **28**, 6741 (1983).
[3] M. Alden, S. Mirbt, H. L. Skriver, N. M. Rosengaard, and B. Johansson, Phys. Rev. B **46**, 6303 (1992).
[4] M. Bender *et al.*, J. Phys. Condens. Matter **7**, 5289 (1995).
[5] S. E. Apsel, J. W. Emmert, J. Deng, and L. A. Bloomfield, Phys. Rev. Lett. **76**, 1441 (1996).
[6] M. A. Ruderman and C. Kittel, Phys. Rev. **96**, 99 (1954).
[7] T. Kasuya, Prog. Theor. Phys. **16**, 45 (1956).

[8] K. Yosida, Phys. Rev. **106**, 893 (1957).
[9] A. Freeman and C. Fu, J. Appl. Phys. **61**, 3356 (1987).
[10] O. Eriksson, A. M. Boring, R. C. Albers, G. W. Fernando, and B. R. Cooper, Phys. Rev. B **45**, 2868 (1992).
[11] I. M. Billas, A. Chatelain, and W. A. de Heer, Science **265**, 1682 (1994).
[12] Y.-W. Son, M. L. Cohen, and S. G. Louie, Nature (London) **444**, 347 (2006).
[13] V. Barone and J. E. Peralta, Nano Lett. **8**, 2210 (2008).
[14] A. R. Botello-Méndez, F. López-Urías, M. Terrones, and H. Terrones, Nano Lett. **8**, 1562 (2008).
[15] Y. Li, Z. Zhou, S. Zhang, and Z. Chen, J. Am. Chem. Soc. **130**, 16739 (2008).
[16] S. C. Erwin and F. Himpsel, Nat. Commun. **1**, 58 (2010).
[17] J. Yu and W. Guo, J. Phys. Chem. Lett. **4**, 1856 (2013).
[18] G. Z. Magda, X. Jin, I. Hagymási, P. Vancsó, Z. Osváth, P. Nemes-Incze, C. Hwang, L. P. Biro, and L. Tapaszto, Nature (London) **514**, 608 (2014).
[19] O. V. Yazyev and L. Helm, Phys. Rev. B **75**, 125408 (2007).
[20] O. V. Yazyev, Phys. Rev. Lett. **101**, 037203 (2008).
[21] C. Jin, F. Lin, K. Suenaga, and S. Iijima, Phys. Rev. Lett. **102**, 195505 (2009).
[22] O. V. Yazyev and M. I. Katsnelson, Phys. Rev. Lett. **100**, 047209 (2008).
[23] D. Yu, E. M. Lupton, H. Gao, C. Zhang, and F. Liu, Nano Res. **1**, 497 (2008).
[24] H. Fu, Z. Liu, C. Lian, J. Zhang, H. Li, J.-T. Sun, and S. Meng, Phys. Rev. B **94**, 035427 (2016).
[25] I. S. Elfimov, S. Yunoki, and G. A. Sawatzky, Phys. Rev. Lett. **89**, 216403 (2002).
[26] S. Gallego, J. Beltrán, J. Cerdá, and M. Munoz, J. Phys.: Condens. Matter **17**, L451 (2005).
[27] I. Shein and A. Ivanovskii, Phys. Lett. A **371**, 155 (2007).
[28] K. Janicka, J. P. Velev, and E. Y. Tsymbal, J. Appl. Phys. **103**, 07B508 (2008).
[29] H. Wu, A. Stroppa, S. Sakong, S. Picozzi, M. Scheffler, and P. Kratzer, Phys. Rev. Lett. **105**, 267203 (2010).
[30] G. Fischer, N. Sanchez, W. Adeagbo, M. Lüders, Z. Szotek, W. M. Temmerman, A. Ernst, W. Hergert, and M. C. Muñoz, Phys. Rev. B **84**, 205306 (2011).
[31] N. Sanchez, S. Gallego, and M. C. Muñoz, Phys. Rev. Lett. **101**, 067206 (2008).
[32] H. Peng, H. J. Xiang, S.-H. Wei, S.-S. Li, J.-B. Xia, and J. Li, Phys. Rev. Lett. **102**, 017201 (2009).
[33] N. Sanchez, S. Gallego, J. Cerdá, and M. C. Muñoz, Phys. Rev. B **81**, 115301 (2010).
[34] T. Cao, Z. Li, and S. G. Louie, Phys. Rev. Lett. **114**, 236602 (2015).
[35] P. Lunkenheimer, J. Muller, S. Krohns, F. Schrettle, A. Loidl, B. Hartmann, R. Rommel, M. de Souza, C. Hotta, J. A. Schlueter *et al.*, Nat. Mater. **11**, 755 (2012).
[36] S.-i. Ohkoshi, Y. Hamada, T. Matsuda, Y. Tsunobuchi, and H. Tokoro, Chem. Mater. **20**, 3048 (2008).
[37] J. Coey, K. Wongsaprom, J. Alaria, and M. Venkatesan, J. Phys. D **41**, 134012 (2008).
[38] Y. Cai, Q. Ke, G. Zhang, and Y.-W. Zhang, J. Phys. Chem. C **119**, 3102 (2015).
[39] J. Hoffman, I. C. Tung, B. B. Nelson-Cheeseman, M. Liu, J. W. Freeland, and A. Bhattacharya, Phys. Rev. B **88**, 144411 (2013).
[40] N. A. Spaldin and M. Fiebig, Science **309**, 391 (2005).
[41] D. N. Astrov, Sov. Phys. JETP **13**, 729 (1961).
[42] M. Fiebig, J. Phys. D **38**, R123 (2005).
[43] K. Wang, J.-M. Liu, and Z. Ren, Adv. Phys. **58**, 321 (2009).
[44] C.-G. Duan, J. P. Velev, R. F. Sabirianov, Z. Zhu, J. Chu, S. S. Jaswal, and E. Y. Tsymbal, Phys. Rev. Lett. **101**, 137201 (2008).
[45] C.-G. Duan, C.-W. Nan, S. S. Jaswal, and E. Y. Tsymbal, Phys. Rev. B **79**, 140403 (2009).
[46] Z. Zhang, C. Chen, and W. Guo, Phys. Rev. Lett. **103**, 187204 (2009).
[47] C.-G. Duan, S. S. Jaswal, and E. Y. Tsymbal, Phys. Rev. Lett. **97**, 047201 (2006).
[48] W. Eerenstein, M. Wiora, J. Prieto, J. Scott, and N. Mathur, Nat. Mater. **6**, 348 (2007).
[49] S. Sahoo, S. Polisetty, C.-G. Duan, S. S. Jaswal, E. Y. Tsymbal, and C. Binek, Phys. Rev. B **76**, 092108 (2007).
[50] F. Zavaliche, T. Zhao, H. Zheng, F. Straub, M. Cruz, P.-L. Yang, D. Hao, and R. Ramesh, Nano Lett. **7**, 1586 (2007).
[51] J. M. Rondinelli, M. Stengel, and N. A. Spaldin, Nat. Nanotech. **3**, 46 (2008).
[52] T. Kimura, T. Goto, H. Shintani, K. Ishizaka, T.-h. Arima, and Y. Tokura, Nature (London) **426**, 55 (2003).
[53] W. Eerenstein, N. Mathur, and J. F. Scott, Nature (London) **442**, 759 (2006).
[54] M. Bibes and A. Barthélémy, Nat. Mater. **7**, 425 (2008).
[55] A. Ohtomo, D. Muller, J. Grazul, and H. Y. Hwang, Nature (London) **419**, 378 (2002).
[56] A. Ohtomo and H. Hwang, Nature (London) **441**, 120 (2006).
[57] A. Brinkman *et al.*, Nat. Mater. **6**, 493 (2007).
[58] R. Oja *et al.*, Phys. Rev. Lett. **109**, 127207 (2012).
[59] Z. Zhang and W. Guo, Nano Lett. **12**, 3650 (2012).
[60] J. Blakemore, J. Appl. Phys. **53**, R123 (1982).
[61] H. Ohno, Science **281**, 951 (1998).
[62] H. Zaari, M. Boujnah, H. Labrim, B. Khalil, A. Benyoussef, and A. El Kenz, J. Supercond. Novel Magn. **26**, 2961 (2013).
[63] H. Ohno, A. Shen, F. Matsukura, A. Oiwa, A. Endo, S. Katsumoto, and Y. Iye, Appl. Phys. Lett. **69**, 363 (1996).
[64] T. Hayashi, M. Tanaka, T. Nishinaga, H. Shimada, H. Tsuchiya, and Y. Otuka, J. Cryst. Growth **175**, 1063 (1997).
[65] S. Das Sarma, E. H. Hwang, and A. Kaminski, Phys. Rev. B **67**, 155201 (2003).
[66] T. Dietl, Nat. Mater. **9**, 965 (2010).
[67] M. R. Mahani, A. Pertsova, and C. M. Canali, J. Phys. Condens. Matter **26**, 394006 (2014).
[68] M. R. Mahani, M. F. Islam, A. Pertsova, and C. M. Canali, Phys. Rev. B **89**, 165408 (2014).
[69] J. Wenisch *et al.*, Phys. Rev. Lett. **99**, 077201 (2007).
[70] G. Kresse and J. Furthmüller, Phys. Rev. B **54**, 11169 (1996).
[71] G. Kresse and J. Furthmüller, Comput. Mater. Sci. **6**, 15 (1996).
[72] D. Vanderbilt, Phys. Rev. B **41**, 7892 (1990).
[73] H. J. Monkhorst and J. D. Pack, Phys. Rev. B **13**, 5188 (1976).
[74] J. Neugebauer and M. Scheffler, Phys. Rev. B **46**, 16067 (1992).
[75] L. Bengtsson, Phys. Rev. B **59**, 12301 (1999).
[76] See Supplemental Material at http://link.aps.org/supplemental/10.1103/PhysRevB.96.184430 for structural properties of GaAs nanofilms, the projected density of states of the outmost As $4p_y$ orbit of ⟨100⟩ nanofilm, the magnetoelectric effect in GaAs⟨100⟩ nanofilms, and the thickness effect on the surface magnetism of GaAs⟨100⟩ nanofilms.

[77] H. L. Zhuang, A. K. Singh, and R. G. Hennig, Phys. Rev. B **87**, 165415 (2013).
[78] C. L. Freeman, F. Claeyssens, N. L. Allan, and J. H. Harding, Phys. Rev. Lett. **96**, 066102 (2006).
[79] D. Wu, M. G. Lagally, and F. Liu, Phys. Rev. Lett. **107**, 236101 (2011).
[80] N. Sivadas, H. Dixit, V. R. Cooper, and D. Xiao, Phys. Rev. B **89**, 075303 (2014).
[81] N. Sivadas, M. W. Daniels, R. H. Swendsen, S. Okamoto, and D. Xiao, Phys. Rev. B **91**, 235425 (2015).
[82] B. Huang *et al.*, Nature (London) **546**, 270 (2017).
[83] M. A. McGuire, H. Dixit, V. R. Cooper, and B. C. Sales, Chem. Mater. **27**, 612 (2015).
[84] W.-B. Zhang, Q. Qu, P. Zhu, and C.-H. Lam, J. Mater. Chem. C **3**, 12457 (2015).